Observing Geometry of Quantum States in a Three-Level System

Jie Xie,[1,2‡] Aonan Zhang,[1,2‡] Ningping Cao,[3,4] Huichao Xu,[1,2] Kaimin Zheng,[1,2] Yiu-Tung Poon,[5] Nung-Sing Sze,[6] Ping Xu,[1,2,7] Bei Zeng,[8,*] and Lijian Zhang[1,2,†]

[1]*National Laboratory of Solid State Microstructures, Key Laboratory of Intelligent Optical Sensing and Manipulation (Ministry of Education), College of Engineering and Applied Sciences and School of Physics, Nanjing University, Nanjing 210093, China*

[2]*Collaborative Innovation Center of Advanced Microstructures, Nanjing University, Nanjing 210093, China*

[3]*Department of Mathematics & Statistics, University of Guelph, Guelph N1G 2W1, Ontario, Canada*

[4]*Institute for Quantum Computing, University of Waterloo, Waterloo N2L 3G1, Ontario, Canada*

[5]*Department of Mathematics, Iowa State University, Ames, Iowa 50011, USA*

[6]*Department of Applied Mathematics, The Hong Kong Polytechnic University, 999077 Hong Kong, China*

[7]*Institute for Quantum Information & State Key Laboratory of High Performance Computing, College of Computer, National University of Defense Technology, Changsha 410073, China*

[8]*Department of Physics, The Hong Kong University of Science and Technology, Clear Water Bay, Kowloon, 999077 Hong Kong, China*

(Received 26 March 2020; accepted 2 September 2020; published 8 October 2020)

In quantum mechanics, geometry has been demonstrated as a useful tool for inferring nonclassical behaviors and exotic properties of quantum systems. One standard approach to illustrate the geometry of quantum systems is to project the quantum state space onto the Euclidean space via measurements of observables on the system. Despite the great success of this method in studying two-level quantum systems (qubits) with the celebrated Bloch sphere representation, it is still difficult to reveal the geometry of multidimensional quantum systems. Here we report the first experiment measuring the geometry of such projections beyond the qubit. Specifically, we observe the joint numerical ranges of a triple of observables in a three-level photonic system, providing a complete classification of these ranges. We further show that the geometry of different classes reveals ground-state degeneracies of a Hamiltonian as a linear combination of the observables, which is related to quantum phases in the thermodynamic limit. Our results offer a versatile geometric approach for exploring the properties of higher-dimensional quantum systems.

DOI: 10.1103/PhysRevLett.125.150401

Arising from Euclid's first attempt to establish its axiomatic form, geometry has become an essential method for understanding the physical world, especially in the field of quantum physics [1–4]. One exemplary use of geometric method was the creation of statistical mechanics in the 1870s, when Gibbs introduced a geometric means to infer thermodynamic properties (e.g., energy or entropy) of a system by considering a convex body constituted by all possible values of physical quantities [5]. Shifting to systems in which the behaviors are governed by quantum physics, the possible expectation values of physical quantities are instead acquired over the entire space of quantum states, mathematically the set of all semidefinite matrices of trace one $\mathcal{M}_d = \{\rho : \rho \geq 0, \mathrm{Tr}(\rho) = 1\}$ in a d-dimensional Hilbert space. The convex body formed by joint expectation values of different observables on all quantum states can be used as a geometric representation of quantum state space. One of the most successful examples is the Bloch sphere of qubit state space [6], which has become the fundamental model in quantum information [7]. Many works are devoted to studying the geometry of higher-dimensional systems, such as generalizing the Bloch vector [6,8–10] and visualizing a single qutrit state [11]. However, there is no satisfactory geometric ways to visualize the whole higher-dimensional state space, which possesses properties dissimilar to those of qubits that are starting to play indispensable roles in quantum information processing [12–14].

In this Letter, we investigate the geometry of quantum states by projecting the state space $\mathcal{M}_d$ onto the n-dimensional Euclidean space $\mathbb{R}^n$ via measurements of n observables on the system [15–18]. This geometric construction allows the exploration of the complicated structure and physical properties of high-dimensional quantum systems through their lower-dimensional projections. Behind this construction is the concept of the numerical range in mathematical terminology. Back in 1918, Toeplitz [15] introduced the numerical range of a $d \times d$ complex matrix F, which is defined as $W(F) = \{z = \langle\psi|F|\psi\rangle : |\psi\rangle \in \mathbb{C}^d, \langle\psi|\psi\rangle = 1\}$. Here $F = F_1 + iF_2$ involves two Hermitian matrices F_1 and F_2. The conjecture by Toeplitz that $W(F)$ is convex was later proved by Hausdorff in 1919 [15,16]. A natural extension, termed the

joint numerical range (JNR) [18], involves a collection of Hermitian matrices $\mathcal{F} = \{F_1, \ldots, F_n\}$,

$$W(\mathcal{F}) = \{(\langle\psi|F_1|\psi\rangle, \ldots, \langle\psi|F_n|\psi\rangle) : |\psi\rangle \in \mathbb{C}^d, \langle\psi|\psi\rangle = 1\}, \quad (1)$$

that naturally form a geometric object in $\mathbb{R}^n$. Then the state space projection via these matrices, which allows the statistical mixture of pure states $|\psi\rangle$, is simply the convex hull of the JNR

$$L(\mathcal{F}) = \{[\mathrm{Tr}(\rho F_1), \ldots, \mathrm{Tr}(\rho F_n)] : \rho \in \mathcal{M}_d\}. \quad (2)$$

In the following, we are mainly concerned with the set $L(\mathcal{F})$ and do not distinguish it from $W(\mathcal{F})$ (see Supplemental Material, Sec. I A [19]).

In recent years, the topic of the numerical range has been reviewed in the study of quantum phase transitions [25–28], the derivation of uncertainty relations [29] and entanglement criterion [30], and error correcting codes in quantum computing [31,32]. Yet many characteristics of JNRs are still unknown for dimensions as low as 3. Recently, Szymański, Weis, and Życzkowski made a crucial step toward resolving this problem by proving the complete classification of the JNR in the case $d = n = 3$ [33]. However, experimentally recovering the geometry of a JNR, together with its classification, demands sampling adequate data, which is a nontrivial problem requiring the ability to implement arbitrary unitary operations on a qudit system [34,35]. Here we perform the first experiment allowing the complete observation of state space projections beyond qubit systems.

As mentioned above, a simple example in a qubit system is the JNR of three Pauli operators known as the Bloch sphere [6], whereas the JNR of other Hermitian matrices is equivalent to a transformation of the Bloch sphere, as shown in Fig. 1(a). Extended to higher-dimensional systems, the geometry of the JNR is associated with a class of system Hamiltonians $H(\vec{h}) = \sum h_i F_i$ parameterized by $\vec{h} = (h_1, \ldots, h_n)$ in the basis $\mathcal{F}$. It is intuitive that surface points (extreme points) of the JNR are generated by ground states of $H(\vec{h})$ (see Supplemental Material, Sec. I B [19]). Geometrically, each parameter vector $\vec{h}$ represents a inward-pointing unit vector in $\mathbb{R}^n$ and corresponds to a supporting hyperplane Π tangent to the surface of the JNR, as depicted in Fig. 1(b). The tangent point is acquired by the ground state $|\psi_g(\vec{h})\rangle$ of $H(\vec{h})$, while the corresponding ground-state energy E_g can be obtained by projecting the point $[\langle F_1\rangle_{\psi_g(\vec{h})}, \ldots, \langle F_n\rangle_{\psi_g(\vec{h})}]$ onto the $\vec{h}$ direction. When continuously varying the parameter vector $\vec{h}$, the envelope of all supporting hyperplanes constitutes the surface of the JNR, which can be generated by all ground states $|\psi_g(\vec{h})\rangle$. If a flat portion exists on the surface of the JNR at a particular direction $\vec{h}$, the supporting hyperplane will be tangent to the whole portion instead of a single point.

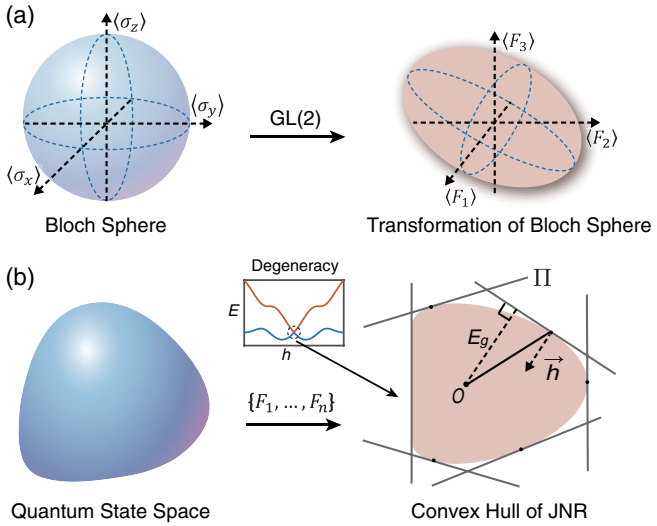

FIG. 1. Quantum state space projection and the joint numerical range (JNR). (a) The state space of a qubit system $\mathcal{M}_2$ can be represented as a Bloch sphere, which is the JNR of the three Pauli operators $\{\sigma_x, \sigma_y, \sigma_z\}$. Undergoing a linear transformation $GL(2)$, the Bloch sphere becomes an ellipsoid as the JNR of three other linearly independent matrices. (b) The state space of a higher-dimensional quantum system ($d \geq 3$) is a convex set with a more complicated structure. Following the qubit case, these structures can be revealed by projecting the state space $\mathcal{M}_d$ to $\mathbb{R}^n$ through a set of n Hermitian observables. This constitutes the convex hull of the JNR, whose surface can be generated by the ground states of a set of system Hamiltonians $H(\vec{h})$ geometrically corresponding to a set of supporting hyperplanes Π (grey, solid lines). In general, ground-state degeneracy happens when a flat portion appears on the surface.

Therefore, this indicates ground-state degeneracy in the sense that different ground states are associated with one system Hamiltonian, $H(\vec{h})$ [28].

In the case $d = n = 3$, the image of the JNR forms a three-dimensional oval that can be classified in terms of its one- or two-dimensional faces, that is, segments or filled ellipses. These faces are invariant under linear transformation and translation. According to the number of segments (s) and filled ellipses (e) on the surface, all the JNRs can be divided into ten possible categories [33]. Among theses, the eight unitarily irreducible categories that we measured are as follows (the other two categories correspond to reducible operator sets, which can be derived by lower-dimensional JNRs; see Supplemental Material, Sec. II D [19]):

$$s = 0; e = 0, 1, 2, 3, 4 \quad \text{and} \quad s = 1; e = 0, 1, 2.$$

To measure the JNR, one can prepare identical copies of quantum states and obtain a triple of expectation values of $\mathcal{F}$ by separately measuring each of the three observables on the same states. Experimentally, qutrit states can be encoded in the photons' different degrees of freedom

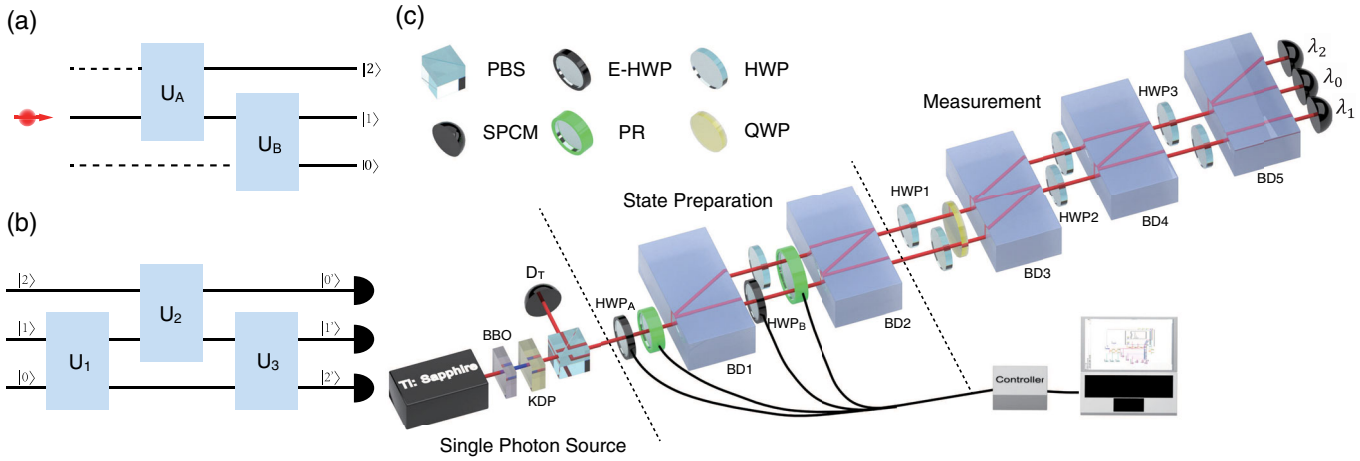

FIG. 2. Experimental scheme. (a) Preparation of single photonic qutrit state. A single photon propagating in three modes represents a three-level quantum system. Sequential two-mode unitary operations can evolve the system to an arbitrary superposition of the three levels. (b) Measurement of a Hermitian observable F_i. The three-outcome measurement, consisting of three two-modes unitary transformations and single-photon detections, projects input states onto the three eigenstates of the observable F_i. (c) Experimental setup. Photon pairs are generated through the parametric downconversion process in a phase-matched potassium di-hydrogen phosphate (KDP) crystal pumped by frequency-doubled Ti:Sapphire laser pulses and then separated by a polarizing beam splitter (PBS). A single photon in the transmitted path is heralded by detection of a reflected photon at the heralding detector D_T. The state preparation module is composed of two electronically controlled half-wave plates (E-HWPs), two phase retarders (PRs), and two calcite beam displacers (BDs). The measurement part is composed of wave plates, BDs, and three single-photon counting modules (SPCMs). For some observables, a quarter-wave plate (QWP) is inserted before BD3. Unlabeled HWPs are set to 45° or 0°.

[36–39]. Here we prepare a single photon in the superposition of three modes that is equivalent to a three-level system such as a spin-one particle. The single photon, generated in a heralded manner by the parametric down-conversion process, is initially injected into one of the three modes. Then after two sequential two-mode unitary operations [Fig. 2(a)], the system is prepared in any pure superposition of the three levels of the form $|\psi\rangle = \cos\theta_1 e^{i\phi_1}|0\rangle + \sin\theta_1 \sin\theta_2 e^{i\phi_2}|1\rangle + \sin\theta_1 \cos\theta_2|2\rangle$. This operation is realized by the state preparation module in Fig. 2(c), which involves wave plates together with a calcite beam displacer to distribute the single photons among three optical modes and two variable phase retarders to manipulate phases between different modes. The three optical modes are defined as the horizontal and vertical polarizations of a single path mode (top) and the vertical polarization (the horizon polarization is not used) of another path mode (lower). The measurement of any Hermitian observable [Fig. 2(b)] is realized by a three-outcome quantum measurement collapsing the state onto one of the three eigenstates of the observable F_i. The state first undergoes a unitary evolution consisting of three sequential two-mode unitaries, so that the input state is transformed in the eigenbasis of the observable F_i [34]. This transformation is accomplished by three cascaded interferometers formed by a set of wave plates and calcite beam displacers, as shown in the measurement part of Fig. 2(c). At the end, three single-photon counting modules are used for the detection of single photons. Clicks of the three detectors indicate measuring the corresponding eigenvalues $\lambda_j^{(i)}$ $(j = 0, 1, 2)$ of F_i, so that the expectation values of F_i can be estimated through the measured probability distribution $\{p_j\}$. The wave plates in the measurement stage can be configured in different settings, thus enabling measurements of different observables with respect to the same set of states.

For each class of the JNR, we provide an example of the 3-tuple of observables $\mathcal{F}$ (see Supplemental Material, Sec. II B [19]) being measured in our experiment. Given that the set of the JNR is convex for $n = 3$ [40] and any interior point can be obtained by the mixture of surface states, measuring pure surface states is enough for the observation of the JNR. We randomly sample 300 ground states $|\psi_g(\theta,\phi)\rangle$ of system Hamiltonians

$$H(\theta,\phi) = \sin\theta\cos\phi F_1 + \sin\theta\sin\phi F_2 + \cos\theta F_3 \qquad (3)$$

for each class (see Supplemental Material, Sec. II A [19]). Here (θ,ϕ) defines the unit vector $\vec{h} = (\sin\theta\cos\phi, \sin\theta\sin\phi, \cos\theta)$. Then we measure the expectation values of the three observables with respect to these ground states. Figure 3 illustrates the experimental results for the exemplary JNRs of eight classes. The experimental results are in line with the theoretical predictions, as they are very close to the surface of the theoretical predictions. The average similarity S between experimentally measured probability distributions $\{p_j\}$ and the theoretical values $\{p_j^{th}\}$ is above 0.994, with $S = \left(\sqrt{p_0 p_0^{th}} + \sqrt{p_1 p_1^{th}} + \sqrt{p_2 p_2^{th}}\right)^2$. The

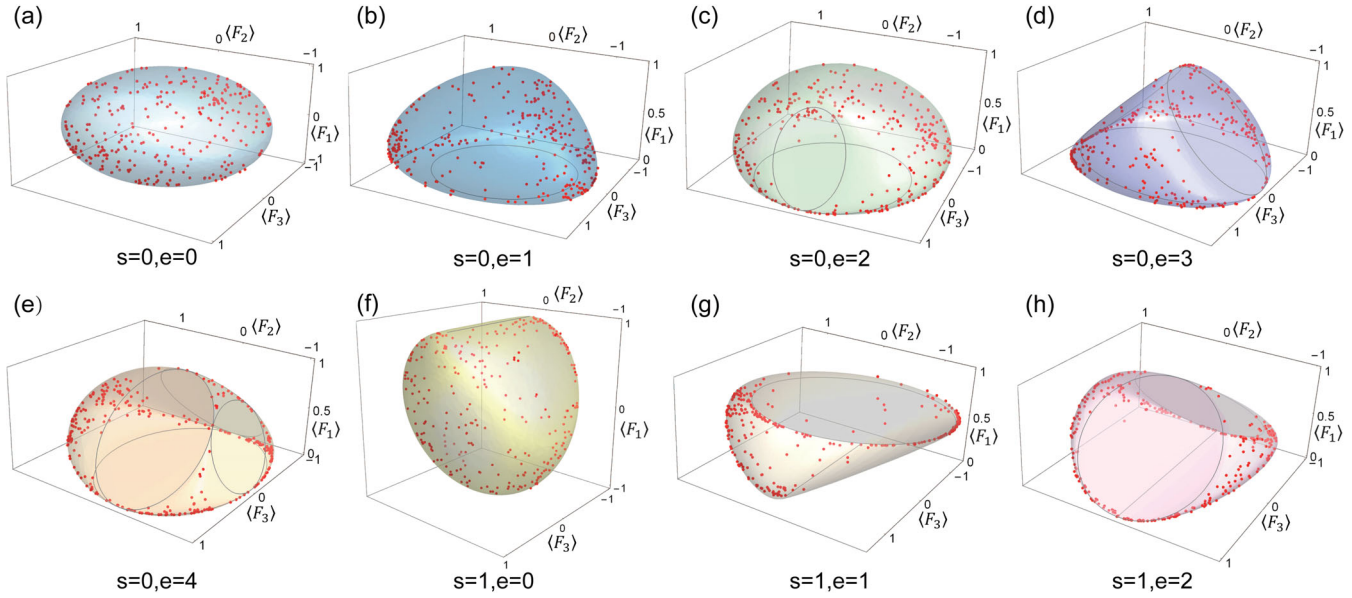

FIG. 3. Complete observation of the JNR. (a)–(h) Experimentally measured data (red dots) and the theoretical predictions of the JNR (chromatic convex bodies) for the examples of the eight possible classes. Each class is specified by the number of segments (s) and filled ellipses (e) on the surface (plotted with gray lines) of the convex body. The experimental data are obtained by measuring the surface states (ground states) of the system Hamiltonians [Eq. (3)]. For each class, 300 surface states are sampled. The theoretical bodies are plotted by sampling adequate ground states (more than 3000 for each class) and then generating the convex hull of the corresponding theoretical points of the JNR.

convex hulls of the experimental data also show the same geometrical features (the number of s and e). Deviations between the observed data and the theoretical values are mainly attributed to systematic errors in the settings of experimental parameters (see Supplemental Material, Sec. II E [19]). Apart from the first class, the remaining seven classes of the JNR are different from either a sphere or an ellipsoid, showing distinct properties of qutrit state space from those of qubits.

Following the complete observation of the geometric bodies, we show how the geometry of JNRs in Fig. 3 determines the ground-state energies and degeneracies of the system Hamiltonians. In Fig. 4, by combining all the experimental results $(\langle F_1\rangle, \langle F_2\rangle, \langle F_3\rangle)$ of $\mathcal{F}$ with their

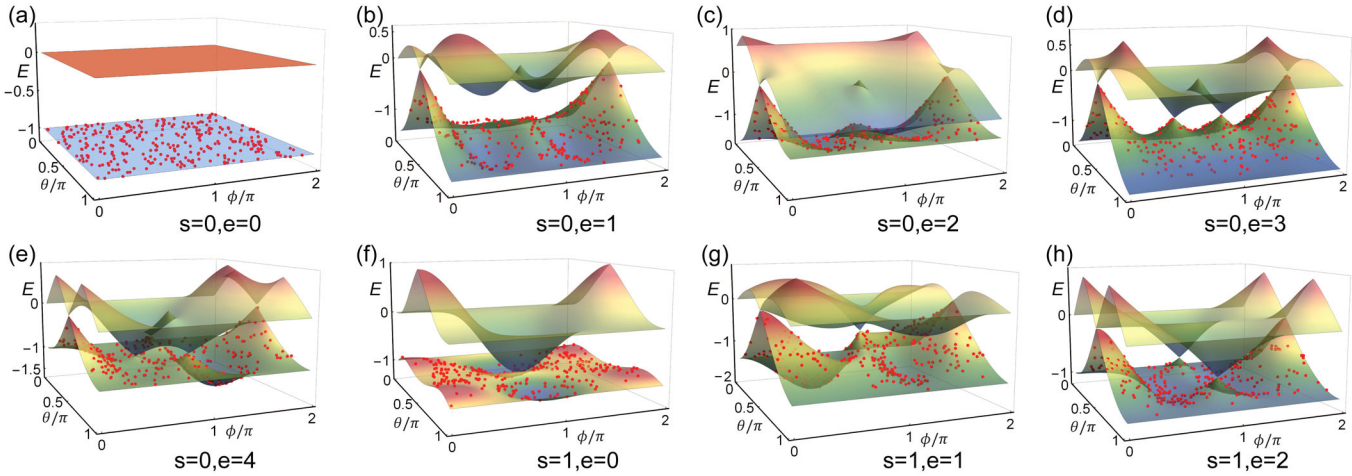

FIG. 4. Determining ground-state energy and degeneracy. (a)–(h) The band structures of the lowest two bands for the system Hamiltonians of the eight JNR classes. Colored surfaces represent the theoretical energy of the ground state and the first excited state of the Hamiltonian $H(\theta, \phi)$ [Eq. (3)] for varied θ, ϕ. The experimental results (red dots) are computed by the experimental data of each class of JNR as indirectly measured expectation values of $H(\theta, \phi)$. The number and features of degeneracy points shown in the band structure diagrams have a correspondence with the number of segments and ellipses on the surfaces of the JNR.

corresponding unit vector (θ, ϕ), we obtain the expectation value E of the system Hamiltonian $H(\theta, \phi)$ and give the diagrams of E (red dots) versus θ and ϕ. The resulting energies are in line with the theoretical prediction of ground-state energies (the lower colored surfaces) within experimental errors. In particular, there is a clear correspondence between the segments and ellipses in Fig. 3 and the degeneracy points in Fig. 4. For example, the first class [Fig. 4(a)] corresponds to a gaped Hamiltonian and there is no flat portion on the surface of its JNR. As for the case $s = 1$, $e = 2$, there are three degeneracy points in the band structure diagram. Two are cone-shaped, which are nonanalytic in all directions and correspond to the two ellipses on the JNR. The other is Λ-shaped, which is nonanalytic only in one direction and corresponds to the segment. These various band structure diagrams, which can be geometrically revealed by the surfaces of the JNRs, also show the distinct features of three-level quantum systems compared to two-level systems.

For quantum matters at the zero temperature, the ground states associated with a class of Hamiltonians are regarded as "quantum phases" of the matter. The degeneracy of ground states, usually indicating a gap closing, is an important indicator of different quantum phases [41] such as symmetry-breaking, topological-ordered, and gapless phases. As demonstrated in our experiment, the flat surfaces (ellipses and segments in the case $d = n = 3$) on an image of the JNR indicate ground-state degeneracies of the Hamiltonian $H(\vec{h})$ and thus represent different phases of the system. Therefore, the surface of the JNR can be viewed as an intuitive geometric representation of quantum phases on which different regions represent different phases.

We experimentally identify the geometry of a three-level quantum system by observing the complete classification of the JNRs of three observables. The results highlight the distinct difference between high-dimensional quantum systems and qubits. Furthermore, we elucidate the relation between the geometric characters of the JNR and the ground-state degeneracies of the system Hamiltonians. Our work opens an avenue to experimentally explore fascinating phenomena of quantum systems via their state space projections. This geometric method is also applicable to many-body systems when the set of observables happens to be the local Hamiltonians of the system, which may be easier to implement than the global ones [42]. Besides this, the concept of the JNR has shown a wide range of potential applications. As convex sets, JNRs have been adopted in the N-representability problem [26,43] and the quantum marginal problem [44] for visualizing the set of reduced density matrices. In the field of quantum information, JNRs find applications in the derivation of entanglement witnesses [30,45] and uncertainty relations [29,46] and provide theoretical foundations for the self-characterization of quantum devices [47,48]. We expect this versatile concept to promote further investigations in understanding the geometry of quantum systems, inferring intriguing phases and properties of quantum matters, as well as developing novel technologies in quantum information science.

This work was supported by the National Key Research and Development Program of China (Grants No. 2019YFA0308704 and No. 2017YFA0303703), the National Natural Science Foundation of China (Grants No. 11690032, 61975077, 91836303, and 61490711) and the Fundamental Research Funds for the Central Universities (Grant No. 020214380068). N. C. was supported by Natural Sciences and Engineering Research Council (NSERC) of Canada. The research of N.-S. S. was supported by an HK RGC grant (PolyU 15305719). The authors thank Y. Zhao, H. Zhang, and T. Lan for enlightening discussions.

*Corresponding author.
zengb@ust.hk
†Corresponding author.
lijian.zhang@nju.edu.cn
‡These authors contributed equally to this work.

[1] I. Bengtsson and K. Zyczkowski, *Geometry of Quantum States: An Introduction to Quantum Entanglement* (Cambridge University Press, Cambridge, England, 2006).
[2] J. Anandan and Y. Aharonov, Geometry of Quantum Evolution, Phys. Rev. Lett. **65**, 1697 (1990).
[3] M. A. Nielsen, M. R. Dowling, M. Gu, and A. C. Doherty, Quantum computation as geometry, Science **311**, 1133 (2006).
[4] N. Flaschner, B. S. Rem, M. Tarnowski, D. Vogel, D.-S. Luhmann, K. Sengstock, and C. Weitenberg, Experimental reconstruction of the Berry curvature in a Floquet Bloch band, Science **352**, 1091 (2016).
[5] J. W. Gibbs, A method of geometrical representation of the thermodynamic properties of substances by means of surfaces, Trans. Conn. Acad. Arts Sci. **2**, 382 (1873).
[6] G. Kimura, The Bloch vector for N-level systems, Phys. Lett. A **314**, 339 (2003).
[7] M. A. Nielsen and I. L. Chuang, *Quantum Computation and Quantum Information* (Cambridge University Press, Cambridge, 2001).
[8] Arvind, K. S. Mallesh, and N. Mukunda, A generalized Pancharatnam geometric phase formula for three-level quantum systems, J. Phys. A **30**, 2417 (1997).
[9] R. A. Bertlmann and P. Krammer, Bloch vectors for qudits, J. Phys. A **41**, 235303 (2008).
[10] D. Aerts and M. S. de Bianchi, The extended Bloch representation of quantum mechanics and the hidden-measurement solution to the measurement problem, Ann. Phys. (Amsterdam) **351**, 975 (2014).
[11] P. Kurzyński, A. Kołodziejski, W. Laskowski, and M. Markiewicz, Three-dimensional visualization of a qutrit, Phys. Rev. A **93**, 062126 (2016).

[12] B. P. Lanyon, M. Barbieri, M. P. Almeida, T. Jennewein, T. C. Ralph, K. J. Resch, G. J. Pryde, J. L. O'brien, A. Gilchrist, and A. G. White, Simplifying quantum logic using higher-dimensional Hilbert spaces, Nat. Phys. **5**, 134 (2009).

[13] Y. Zhang, F. S. Roux, T. Konrad, M. Agnew, J. Leach, and A. Forbes, Engineering two-photon high-dimensional states through quantum interference, Sci. Adv. **2**, e1501165 (2016).

[14] J. Wang, S. Paesani, Y. Ding, R. Santagati, P. Skrzypczyk, A. Salavrakos, J. Tura, R. Augusiak, L. Mančinska, D. Bacco *et al.*, Multidimensional quantum entanglement with large-scale integrated optics, Science **360**, 285 (2018).

[15] O. Toeplitz, Das algebraische Analogon zu einem Satze von Fejér, Math. Z. **2**, 187 (1918).

[16] F. Hausdorff, Der Wertvorrat einer Bilinearform, Math. Z. **3**, 314 (1919).

[17] C. F. Dunkl, P. Gawron, J. A. Holbrook, J. A. Miszczak, Z. Puchała, and K. Życzkowski, Numerical shadow and geometry of quantum states, J. Phys. A **44**, 335301 (2011).

[18] E. Gutkin and K. Życzkowski, Joint numerical ranges, quantum maps, and joint numerical shadows, Linear Algebra Appl. **438**, 2394 (2013).

[19] See Supplemental Material, which includes Refs. [20–24], at http://link.aps.org/supplemental/10.1103/PhysRevLett.125.150401 for the detailed theoretical information on the JNR and experimental details for the state preparation, measurement of the JNR, and additional experimental results and analysis.

[20] C.-K. Li and Y.-T. Poon, Convexity of the joint numerical range, SIAM J. Matrix Anal. Appl. **21**, 668 (2000).

[21] F. Bonsall and J. Duncan, *Numerical Ranges of Operators on Normed Spaces and of Elements of Normed Algebras* (Cambridge University Press, Cambridge, 1971).

[22] Y.-T. Wang, J.-S. Tang, Z.-Y. Wei, S. Yu, Z.-J. Ke, X.-Y. Xu, C.-F. Li, and G.-C. Guo, Directly Measuring the Degree of Quantum Coherence using Interference Fringes, Phys. Rev. Lett. **118**, 020403 (2017).

[23] R. B. M. Clarke, V. M. Kendon, A. Chefles, S. M. Barnett, E. Riis, and M. Sasaki, Experimental realization of optimal detection strategies for overcomplete states, Phys. Rev. A **64**, 012303 (2001).

[24] D. S. Keeler, L. Rodman, and I. M. Spitkovsky, The numerical range of 3×3 matrices, Linear Algebra Appl. **252**, 115 (1997).

[25] J. Chen, Z. Ji, C.-K. Li, Y.-T. Poon, Y. Shen, N. Yu, B. Zeng, and D. Zhou, Discontinuity of maximum entropy inference and quantum phase transitions, New J. Phys. **17**, 083019 (2015).

[26] V. Zauner, D. Draxler, L. Vanderstraeten, J. Haegeman, and F. Verstraete, Symmetry breaking and the geometry of reduced density matrices, New J. Phys. **18**, 113033 (2016).

[27] J.-Y. Chen, Z. Ji, Z.-X. Liu, Y. Shen, and B. Zeng, Geometry of reduced density matrices for symmetry-protected topological phases, Phys. Rev. A **93**, 012309 (2016).

[28] I. M. Spitkovsky and S. Weis, Signatures of quantum phase transitions from the boundary of the numerical range, J. Math. Phys. (N.Y.) **59**, 121901 (2018).

[29] K. Szymański and K. Życzkowski, Geometric and algebraic origins of additive uncertainty relations, J. Phys. A **53**, 015302 (2020).

[30] J. Czartowski, K. Szymański, B. Gardas, Y. V. Fyodorov, and K. Życzkowski, Separability gap and large-deviation entanglement criterion, Phys. Rev. A **100**, 042326 (2019).

[31] D. W. Kribs, A. Pasieka, M. Laforest, C. Ryan, and M. P. da Silva, Research problems on numerical ranges in quantum computing, Linear Multilinear Algebra **57**, 491 (2009).

[32] C.-K. Li and Y.-T. Poon, Generalized numerical ranges and quantum error correction, J. Oper. Theory **66**, 335 (2011), http://www.jstor.org/stable/24715998.

[33] K. Szymański, S. Weis, and K. Życzkowski, Classification of joint numerical ranges of three hermitian matrices of size three, Linear Algebra Appl. **545**, 148 (2018).

[34] M. Reck, A. Zeilinger, H. J. Bernstein, and P. Bertani, Experimental Realization of Any Discrete Unitary Operator, Phys. Rev. Lett. **73**, 58 (1994).

[35] J. Carolan, C. Harrold, C. Sparrow, E. Martín-López, N. J. Russell, J. W. Silverstone, P. J. Shadbolt, N. Matsuda, M. Oguma, M. Itoh, G. D. Marshall, M. G. Thompson, J. C. F. Matthews, T. Hashimoto, J. L. O'Brien, and A. Laing, Universal linear optics, Science **349**, 711 (2015).

[36] A. Vaziri, J.-W. Pan, T. Jennewein, G. Weihs, and A. Zeilinger, Concentration of Higher Dimensional Entanglement: Qutrits of Photon Orbital Angular Momentum, Phys. Rev. Lett. **91**, 227902 (2003).

[37] Y. I. Bogdanov, M. V. Chekhova, L. A. Krivitsky, S. P. Kulik, A. N. Penin, A. A. Zhukov, L. C. Kwek, C. H. Oh, and M. K. Tey, Statistical reconstruction of qutrits, Phys. Rev. A **70**, 042303 (2004).

[38] Z. E. D. Medendorp, F. A. Torres-Ruiz, L. K. Shalm, G. N. M. Tabia, C. A. Fuchs, and A. M. Steinberg, Experimental characterization of qutrits using symmetric informationally complete positive operator-valued measurements, Phys. Rev. A **83**, 051801(R) (2011).

[39] R. Lapkiewicz, P. Li, C. Schaeff, N. K. Langford, S. Ramelow, M. Wieśniak, and A. Zeilinger, Experimental non-classicality of an indivisible quantum system, Nature (London) **474**, 490 (2011).

[40] Y. Au-Yeung and Y. Poon, A remark on the convexity and positive definiteness concerning Hermitian matrices, Southeast Asian Bull. Math. **3**, 85 (1979).

[41] X. G. Wen and Q. Niu, Ground-state degeneracy of the fractional quantum Hall states in the presence of a random potential and on high-genus Riemann surfaces, Phys. Rev. B **41**, 9377 (1990).

[42] C. Kokail, C. Maier, R. van Bijnen, T. Brydges, M. K. Joshi, P. Jurcevic, C. A. Muschik, P. Silvi, R. Blatt, C. F. Roos, and P. Zoller, Self-verifying variational quantum simulation of lattice models, Nature (London) **569**, 355 (2019).

[43] R. M. Erdahl, The Convex Structure of the Set of N-Representable Reduced 2-Matrices, J. Math. Phys. (N.Y.) **13**, 1608 (1972).

[44] A. A. Klyachko, Quantum marginal problem and N-representability, J. Phys. Conf. Ser. **36**, 72 (2006).

[45] C. Branciard, D. Rosset, Y.-C. Liang, and N. Gisin, Measurement-Device-Independent Entanglement Witnesses for All Entangled Quantum States, Phys. Rev. Lett. **110**, 060405 (2013).

[46] R. Schwonnek, L. Dammeier, and R. F. Werner, State-Independent Uncertainty Relations and Entanglement Detection in Noisy Systems, Phys. Rev. Lett. **119**, 170404 (2017).

[47] H. Ren and Y. Li, Modeling Quantum Devices and the Reconstruction of Physics in Practical Systems, Phys. Rev. Lett. **123**, 140405 (2019).

[48] A. Zhang, J. Xie, H. Xu, K. Zheng, H. Zhang, Y.-T. Poon, V. Vedral, and L. Zhang, Experimental Self-Characterization of Quantum Measurements, Phys. Rev. Lett. **124**, 040402 (2020).